

Responses

We thank reviewer and editor for their kind help in improving the manuscript. All the suggested modifications have been made in the submitted manuscript.

Because the modifications were mostly technical in nature related to language and formatting, we are not providing point-by-point reply.

Once again we take this as an opportunity to thank both reviewers and editors for their help and encouragement.

1 **Response of OH airglow emissions to the mesospheric gravity waves and its**
2 **comparisons with full wave model simulation at a low latitude Indian station**

3

4 **R. N. Ghodpage¹, M. P. Hickey², A. Taori^{3,4}, Devendraa Siingh⁵ and P. T. Patil¹**

5

6 [1] {Indian Institute of Geomagnetism, Shivaji University Campus, Kolhapur 416004, India}

7 [2] {Embry-Riddle Aeronautical University, FL - 32114, USA}

8 [3] {National Atmospheric Research Laboratory, Pakala Mandal, Gadanki (A. P.) 517112,
9 India}

10 [4] {now at- National Remote Sensing Center (NRSC), Hyderabad, 500037, India}

11 [5] {Indian Institute of Tropical Meteorology, Pune-411 008, Maharashtra, India}

12

13

14 **Abstract:**

15 The quasi-monochromatic gravity wave induced oscillations, monitored using the mesospheric
16 OH airglow emission over Kolhapur (16.8°N and 74.2°E), India during January to April 2010
17 and January to December 2011, have been characterized using the Krassovsky method. The
18 nocturnal variability reveals prominent wave signatures with periods ranging from 5.2-10.8 hr as
19 the dominant nocturnal wave with embedded short period waves having wave periods 1.5-4.4 hr.
20 The results show that the magnitude of the Krassovsky parameter, viz., $|\eta|$ ranged from 2.1 to
21 10.2 for principal or long nocturnal waves (5.2 to 10.8 hr observed periods), and, from 1.5 to 5.4
22 for the short waves (1.5 to 4.4 hr observed periods) during the years of 2010 and 2011,
23 respectively. The phase, i.e., Φ values of the Krassovsky parameters exhibited larger variability
24 and varied from -8.1° to -167° . The deduced mean vertical wavelengths are found to be
25 approximately -60.2 ± 20 km and -42.8 ± 35 km for long and short wave periods for the year
26 2010. Similarly, for 2011 the mean vertical wavelengths are found to be approximately $-77.6 \pm$
27 30 km and -59.2 ± 30 km for long and short wave periods, respectively, indicating that the
28 observations over Kolhapur were dominated by upward propagating waves. We use a full wave
29 model to simulate the response of OH emission to the wave motion and compare the results with
30 observed values. ~~We discuss the observed wave characteristics and cause of the noted~~

31 ~~differences.~~

32 **Keywords:** OH emissions, Mesospheric gravity wave, Full wave model

33 1. Introduction

34 The airglow Hydroxyl emissions (OH) have been ~~oftenly widely~~ used for studying atmospheric
35 temperature variation in the mesopause region since the pioneering work of Meinel (1950) and
36 its usefulness to derive ~~(Greet et al., 1998, Bittner et al., 2000)~~. ~~The the OH~~ rotational
37 temperature ~~(Greet et al., 1998, Bittner et al., 2000)~~ ~~is one of useful parameters to monitor such~~
38 ~~variable atmospheric temperature in the mesopause region~~. The collision frequency of OH with
39 the neutral atmosphere in the neighborhood of 90 km of altitude should be in an order to 10^4 s^{-1}
40 and the life time of the excited Hydroxyl emission is around 3 to 10 msec. (Mies, 1974). This
41 ensures that the excited OH molecules in the rotational energy levels are in a thermal equilibrium
42 with the atmospheric ambient gases (Sivjee & Hamwey, 1987, Takahashi et al., 1998). Thus, it is
43 normally assumed that the rotational state of OH band is in Maxwell-Boltzmann distribution.
44 The radiated light intensity provides a direct measure of OH quantum state distribution in the
45 mesopause, ~~if one knows the Einstein coefficients governing the emission~~. Meriweather (1975)
46 arrived at an expression for the P1(2) and P1 (5) rotational lines of OH (8-3) band by making use
47 of the vibration-rotation transition probabilities of Mies (1974). Therefore using two lines from a
48 single band we can estimate the rotational temperature by the given equation (Mies, 1974):

$$49 \quad T_{n,m} = \frac{E_{v'}(J'_m) - E_{v'}(J'_n)}{k \ln \left[\frac{I_n}{I_m} \frac{A(J'_m, v' \rightarrow J''_{m+1}, v'')}{A(J'_n, v' \rightarrow J''_{n+1}, v'')} \frac{2J'_m + 1}{2J'_n + 1} \right]}$$

50 Where $T_{n,m}$ is the rotational temperature calculated from two line intensities, I_n and I_m , from
51 rotational levels J'_n, J'_m in the upper vibrational level v' , to J''_{n+1}, J''_{m+1} in the lower vibrational
52 level v'' . $E_v(J)$ is the energy of the level (J, v) . $A(J'_n, v' \rightarrow J''_{n+1}, v'')$ is the Einstein coefficient,

53 for the transition from J'_n, v' to J''_m, v'' . The intensity ratio between P1 (2) and P1 (5) lines of the
54 OH(8,3) band were used to obtain rotational temperature using the transition probabilities as
55 given by Mies (1974) (~~Stubbs et al., 1983~~). Often the observed temporal variations in the
56 mesospheric hydroxyl OH night airglow intensities and rotational temperatures are caused by
57 propagating gravity waves from the lower to the upper atmosphere.

58 The interaction of these upward propagating waves with the ambient and other waves
59 contribute to the dynamical variability, which in turn is reflected in observed airglow intensity
60 and temperature perturbations (Hines, 1997). Krassovsky (1972) introduced a quantity 'η' to
61 characterize the wave-induced perturbations. This parameter, termed as 'Krassovsky's
62 parameter', is now defined as $\eta = |\eta| e^{-i\Phi}$, where $|\eta|$ indicates the ratio of the amplitude variation
63 between the emission intensity and temperature perturbations normalized to their time averages
64 and Φ is the phase difference between the intensity wave and its temperature counterpart (e.g.,
65 Walterscheid et al., 1987; Taylor et al., 1991). It should also be mentioned ~~here~~ that apart from
66 the pure dynamical processes η can also be affected by various other unknown parameters, such
67 as the variation of local oxygen photochemistry (Hickey et al., 1993) and height variation of the
68 emission layer, which affects emission rates and temperature directly (Liu and Swenson 2003;
69 Vargas et al., 2007). Although this can complicate studies of Krassovsky's parameter, it offers an
70 opportunity to study the above aspects ~~at the same time~~. Overall, once the physics and chemistry
71 of emissions are well understood, the η values would offer a good tool to study the perturbations
72 caused in a parameter (temperature, brightness/intensity) by measuring one under the assumption
73 that gravity wave induced perturbations are of adiabatic conditions nature.

74 Utilizing the above, many investigators have carried out observational as well as ~~the~~
75 theoretical studies on the identification and characterization of gravity wave and tidal signatures

76 with wave periodicities ranging from few minutes to several hours (e.g., Walterscheid et al.,
77 1987; Hecht et al., 1987; Hickey 1988a, b; Taylor et al., 1991; Takahashi et al., 1992; Reisin
78 and Scheer 1996; Taori and Taylor 2006; Guharay et al., 2008; Ghodpage et al., 2012, 2013).
79 However, observational studies of the magnitude and phase of η over a range of wave periods for
80 a given location and season are sparse. Some of the notable observations of η for the OH
81 emission have been performed by Viereck and Deehr (1989) in the wave period range of $\sim 1 - 20$
82 hr and by Reisin and Scheer (1996) near to the semidiurnal tidal fluctuations.

83 In the present work, we utilize the mesospheric OH emission intensity and temperature
84 data obtained during January - April 2010 and January - December 2011, when clear and
85 moonless nights allowed observations to exceed 5 hours duration. We deduce the Krassovsky
86 parameters as a function of observed wave period and also infer the vertical wavelengths for the
87 observed mesospheric waves. Further, we compare our estimates with the earlier results reported
88 by various investigators. We also employ a full-wave model to simulate the effects of wave
89 motions on the OH airglow. This model has been used previously to compare observations and
90 theory of airglow fluctuations (e.g., Hickey et al., 1998; Hickey and Yu 2005). Here, the model
91 is used to estimate the values of the amplitudes and phases of Krassovsky's ratio which are
92 compared to those derived from the observations, making the present study unique **and first of its**
93 **kind over as such model comparison over India has not been done before-Indian latitudes.**

94

95 **2. Instrumentation and Observations**

96

97 The mesospheric OH observations are made using the multispectral photometer from Kolhapur
98 (16.8°N, 74.2°E) (Ghodpage et al., 2013, 2014). We analyze the data from January - April 2010
99 and January-December 2011 when clear sky conditions prevailed for several nights. For the year

100 2010, 13 nights out of 45 nights of observation clearly showed wavelike features, while in 2011,
101 29 from 60 nights of data exhibited wavelike variations.

102

103 **2.1 The multispectral photometer**

104 Regular observations of the night airglow emissions, OI 630.0 nm, OI 557.7nm and OH Meinel
105 (731 nm and 740 nm) band have been carried out at the low latitude station Kolhapur. We have
106 operated multispectral photometer pointing to the zenith over Kolhapur. The filters have a band
107 width of 1 nm and their temperature is controlled by a temperature controller at 24 °C. The
108 temperature coefficient of filter is 0.011 nm/°C. At 24°C the transmission efficiency of filters is
109 40 - 70 %. We kept the integration time for each filter 15 seconds which results in repetition time
110 of 90 seconds with an accuracy of approximately ±0.5% for line intensity. The photometer has
111 F/2 optics with ~~full field of view~~ ~10° full field of view. The stepper motor rotation and sensing
112 of the initial position is performed by computer controlled software. As the detector, the
113 EMI9658B photomultiplier tube is used. An amplifier (high gain trans-impedance) is used to ~~to~~
114 convert and amplify the very weak photomultiplier's very weak output current (in the range of
115 nA) ~~output current~~ in-to corresponding voltage form. In the absence of standard calibration
116 source, we have used relative intensities (arbitrary units). In order to study the wave features
117 present in the MLT region, we consider clear sky nights having more than 5 hours of continuous
118 OH band data as mentioned in earlier reports (e.g., Taori et al., 2005).

119

120 **2.2 Full Wave Model**

121 The full-wave model is a linear, steady-state model that solves the linearized Navier-Stokes
122 equations on a high resolution vertical grid to describe the vertical propagation of acoustic-

123 gravity waves in a windy background atmosphere including molecular viscosity and thermal
124 conduction, ion drag, Coriolis force and the eddy diffusion of heat and momentum in the
125 mesosphere. The model description, including equations, boundary conditions and method of
126 solution has been described elsewhere (Hickey et al., 1997; Walterscheid and Hickey 2001;
127 Schubert et al., 2003). The neutral perturbations are used as input to a linear, steady-state model
128 describing OH airglow fluctuations (Hickey and Yu 2005).

129 The model solves the equations on a high resolution vertical grid subject to boundary
130 | conditions, and allows ~~quite~~ generally for the propagation in a height varying atmosphere (non-
131 | isothermal mean state temperature and height varying mean winds and diffusion). The linearized
132 | equations are numerically integrated from the lower to the upper boundary using the tri-diagonal
133 | algorithm described by Bruce et al. (1958) and Lindzen and Kuo (1969). The lower boundary is
134 | set well below the region of interest and a sponge layer is implemented to avoid effects of wave
135 | reflection in the airglow response. In this study the lower boundary (the bottom of the lower
136 | sponge layer) is placed at 250 km below $z = 0$ (i.e., -250 km). The wave forcing is through the
137 | addition of heat in the energy equation. The heating is defined by a Gaussian profile with a full-
138 | width-at-half-max of 0.125 km. It is centered at an altitude of 10 km. A Rayleigh-Newtonian
139 | sponge layer, in addition to natural absorption by viscosity and heat conduction prevents
140 | spurious reflection from the upper boundary. At the upper boundary (here 300 km altitude) a
141 | radiation condition is imposed using a dispersion equation that includes viscous and thermal
142 | dissipation (Hickey and Cole 1987). The mean state is defined using the Mass Spectrometer
143 | Incoherent Scatter (MSIS) model (Hedin 1991).

144 A set of linear perturbation equations for the minor species involved in the OH emission
145 | chemistry is solved using the approach described in Hickey (1988). This assumes that these

146 minor species have the same velocity and temperature perturbations as the major gas (which are
147 deduced from the full-wave model). A vertical integration of the volume emission rates through
148 the vertical extent of the OH layer provides the brightness and brightness-weighted temperature
149 perturbations, from which Krassovsky's ratio is determined. The OH chemistry we use is the
150 same as that used previously (Hickey et al., 1997) and is for the OH (8-3) emission. We also
151 determine the vertical wavelength at the peak of the OH emission layer evaluated from the phase
152 variations of the temperature perturbations determined by the full-wave model.

153

154 **2.3 Space borne measurements**

155 The Sounding of the Atmosphere using Broadband Emission Radiometry (SABER), on-board
156 the Thermosphere Ionosphere Mesosphere Energetic and Dynamics (TIMED) satellite, is a high-
157 precision broadband radiometer which measures limb radiance (orbital inclination at 74°) of the
158 terrestrial atmosphere ~~at~~ in 10 selected spectral bands ranging from 1.27 to 15 μm . In the present
159 study, we note larger values of $|\eta|$ occur during 2011 compared to 2010 for long/principal
160 waves, which indicates a larger intensity to temperature perturbation ratio over Kolhapur during
161 the passage of the waves during 2011. This could be due to the differences in either the
162 background atmosphere or the dynamical processes. To identify the differences in the OH
163 emission layer in year 2010 and 2011, we scrutinize the OH volume emission rate profile for
164 Kolhapur region (~~obtained from SABER~~) ~~satellite~~. The selected latitude-longitude grids are
165 10°N to 20°N and 70°E to 90°E representing Kolhapur. The criteria for the selection of SABER
166 data are such that: (i) the SABER pass should be during typical observation times (excluding
167 twilight time).

168

169 3. Results and Discussion

170 To identify the wave structures in the data, we utilize the perturbation amplitudes normalized to
171 their time averaged values (hereafter referred to as mean values) in the intensity and temperature
172 data to calculate the Krassovsky ratio. To illustrate this, we show a typical example
173 corresponding to the data obtained on 26-27 January 2011 in Figure 1. We plot the intensity
174 deviations ~~temperature deviations~~ from their mean values in figure 1(a), while, the temperature
175 deviations ~~intensity deviations~~ from their mean values are plotted in figure 1(b). We note that
176 night airglow intensity variations show a long-period wave with embedded short-period
177 oscillatory features. On this night, the mean airglow intensity is found to be ~ 1.83 arbitrary units
178 and the mean temperature data is ~ 195.75 K. To identify the nocturnal variability plotted
179 together with data as solid red lines are the of best-fit cosine model (e.g., Taori et al., 2005) as
180 follows. ~~Also, best fit cosines are shown (solid red lines).~~

$$181 \quad Y = A \cos \left[\pi \frac{(X - X_c)}{T} \right] \quad (1)$$

182 where, A is the amplitude of the fitted wave of half-period T with phase X_c , and X is the time.
183 The solid red lines in figure 1 show the results of the best-fit cosine model. We observed the
184 presence of $\sim 8.2 \pm 1.1$ hr and 8 ± 1.3 hr waves with relative amplitudes (normalized to their
185 mean values and converted to corresponding % amplitude) $\sim 3.6\%$ ~~0 K~~ and 25.64%, in the
186 nocturnal temperature and intensity variability, respectively. Given the uncertainties involved in
187 the observations, we consider these to be the same waves. Further, we compute the $|\eta|$ value for
188 this wave to be 7.12 ± 1.2 . To identify the shorter period features in the data we obtain residuals
189 from the best-fit model values. The figure 1c and 1d panels show the nocturnal variability of the

190 residual intensity and temperature respectively. The best-fit model reveals the presence of ~ 4.2
 191 ± 0.2 and 3.0 ± 0.8 hr wave in the temperature and intensity residuals, respectively. Once again
 192 we treat these as the same wave for the reason explained above. The best-fit analysis shows the
 193 amplitudes of this wave to be ~ 1.019 ~~%K~~ and 3.75% arbitrary units in the temperature and
 194 intensity data, respectively. Hence, the $|\eta|$ value for short period waves is estimated to be 3.68
 195 ± 0.9 . In general we note that in worst case, the maximum error in $|\eta|$ values are $<25\%$. The phase
 196 difference between the intensity and temperature waves is obtained with the help of best-fit
 197 parameters, which were also verified with a cross correlation analysis. The phase of the principal
 198 waves (maxima) (period ~ 8.2 hr) was ~ 24.88 hr in the temperature data and 24.4 hr in the
 199 intensity data, which results in the phase difference of ~ 0.48 hr, i.e., Φ values of $-21.07 \pm 12^\circ$.
 200 Similarly, for the shorter period (period ~ 4.2 hr) the Φ values are estimated to be $-114.3 \pm 20^\circ$.
 201 We can also estimate the vertical wavelength with the help of Krassovsky's parameter following
 202 the approach elaborated by Tarasick & Hines (1990).

$$203 \quad \lambda_z = \frac{2\pi\gamma H}{(\gamma - 1)|\eta| \sin(\phi)} \quad (2)$$

204 where $\gamma = C_p / C_v = 1.4$ is the ratio of specific heats, and $H = 6$ km is the scale height. This
 205 formula is valid for zenith observations and for plane waves. It is not valid for the evanescent
 206 waves. Equation (2), negative vertical wavelength corresponds to downward phase propagation
 207 (i.e., upward energy propagation), and that means that temperature oscillations precede the
 208 intensity oscillations in phase (e.g., Takahashi, ~~H.~~, et al. 1990). Using the above relation we find
 209 that vertical wavelength for the two cases discussed above are $\sim -51.5 \pm 15$ and -39.3 ± 40 km for
 210 the long period and the short period waves, respectively. Note that the long period wave
 211 estimates may be biased when the data length is comparable to that of the wave period and

212 therefore in our study we have considered only those waves whose periods are substantially less
213 than the length of the available data.

214 The above analysis was carried out on nighttime events recorded during 2010 and 2011
215 when the prominent wave features were visible. During the 2010 period, the principal nocturnal
216 waves in the data show the wave periods vary from 5.2 to 10.8 hr with corresponding
217 temperature amplitudes ranging from 2 to 13.8 K. Similarly for 2011, wave periods vary between
218 5.2 and 8.4 hr with corresponding temperature amplitudes lying between 1.1 K and 15.7 K.
219 However, the intensity amplitudes of the principal waves vary from 7.9% to 49.9 % and 5% to
220 90% for 2010 and 2011, respectively. We note that the estimated $|\eta|$ values were found to range
221 from 2.1 - 10.5 for the principal wave. In the case of the short period waves, the periods ranged
222 from 1.5 to 4.4 hr (for 2010) and 2.8 to 4.4 hr (for 2011) with corresponding temperature
223 amplitudes ranging from 0.68 K to 12.2 K and 0.4 K to 14.2 K. The corresponding intensity
224 amplitudes fall in range between $\sim 1.54\%$ to 46.8% and 1.32% to 46.8% for 2010 and 2011,
225 respectively. The phase (Φ) values also exhibit large variability for long (short) period waves,
226 range in between -27° and -167° (-27° and -150°) for 2010 and -8.1° and -65.2° (-39.1° and
227 -122.6°) for 2011. For 2010 the deduced vertical wavelengths are found to vary from -32.2 km
228 to -140 km and -24 km to -88 km for the long and short period waves, respectively. Similarly,
229 for 2011 the deduced vertical wavelengths are found to vary from -40 km to -102 km, and -26
230 km to -92.4 km for the long and short period waves, respectively.

231 In Figure 2a we plot our results for $|\eta|$ (hereafter η) with pink half-filled squares
232 indicating the estimates for the year 2010 and olive half-filled squares for the year 2011. We plot
233 Φ in Figure 2b using the same symbols as used in Figure 2a. For a comparison, we also show the
234 values of η and Φ of the results from other investigations are shown (Viereck and Deehr 1989;

235 Takahashi et al., 1992; Oznovich et al., 1995, 1997; Drob 1996; Reisin and Scheer 1996; Taylor
236 et al., 2001; Lopez-Gonzalez et al., 2005). Also shown in the figure are the model estimates of
237 Schubert et al. (1991), Tarasick and Shepherd (1992a, b), Walterscheid and Schubert (1995). We
238 also plot observed η and Φ values against ~~there~~their observed period in figure (2a1 and 2b1). In
239 general, we note that the parameter η increases with wave period. It is evident that the observed
240 η and Φ values in our study show a large spread in their distribution as compared to the model
241 values. A similar spread in the distribution of observed values of η (Figure 2a) from 1.03 to 7.85
242 has also been observed by other investigators (e.g., Takahashi et al., 1992). It may be noted that
243 the values of η for the OH data in our study lie somewhere between the model estimates and the
244 values observed by other investigators. Also noteworthy in this figure is that our η values are
245 closer to the model values reported by Tarasick and Shepherd (1992a) for the waves with
246 horizontal wavelength 500 km. The observed phase ' Φ ' values, on the other hand show
247 significantly larger deviations from this model for 2010, while for 2011 ~~the match between~~
248 ~~measured and modeled phases~~agreement ~~appear~~seems to be better. We note that our
249 measurements of Φ matches somewhat with those reported by Viereck and Deehr (1989), while
250 large differences with other ~~investigators published results~~ can be easily noted. The variation of
251 Φ values with respect to the wave periodicity, obtained in the 2010 year clearly shows that most
252 of the time we observe values to be higher than those obtained by different models.
253 Of the importance is that Reisin & Scheer (2001) found η values of 3.47 ± 0.07 corresponding to
254 the wave periods between 1000s and 3h. Our observed values of η (arithmetic mean, 4.4 ± 1 for
255 2010 year and 5.7 ± 1.7 for 2011 year) for OH measurements agree well with this report. ~~In a~~
256 ~~further report, based on 5-year observations, Reisin and Scheer (2004), found the mean value of~~
257 ~~η to be ~ 5.6 for the nightly semidiurnal type waves and ~ 3.4 for the waves of 3000 s periodicity~~

258 | ~~which is in agreement with our values.~~—In another study based on long-term observations with a
259 | spectral airglow temperature imager (SATI) from a mid-latitude station, Lopez-Gonzalez et al.
260 | (2005) reported a mean value of η of approximately ~ 8.6 for the OH measurements with a larger
261 | variability than our observations show. In another report, Guharay et al. (2008), found that for
262 | wave periods ranging from 6 hr to 13 hr, values of η ~~is~~ between 1.7 to 5.4, while the phase
263 | varied from -13° to -90° . Similarly, Aushev et al. (2008) presented amplitudes of the
264 | Krassovsky parameter for wave periods of 2.2 to 4.7 hr which in range from 2.4 to 3.6 while the
265 | phase values in between -63° to -121° . It is noteworthy that our derived values broadly agree
266 | with Guharay et al. (2008, 2009), Reisin and Scheer (2001, 2004) and Viereck and Deehr (1989)
267 | while they are somewhat different from the values reported by Lopez-Gonzalez et al. (2005)
268 | which may be due to the fact that their observations corresponded to higher latitude than ours.
269 | ~~because of, it is~~ also remains to be seen that when mesopause altitude itself changes from low to
270 | high latitudes how would that reflects in the Krassovsky parameters.

271 | The results of (η and Φ) shown in Figure 2 emphasize that there are significant
272 | differences in the Krassovsky parameters derived from one study to another. This we suspect to
273 | be caused by the variations in the altitudinal profile of oxygen and its effect on the η through the
274 | complex OH chemistry (Walterscheid et al., 1994). Another possibility over low latitudes was
275 | discussed by Makhlouf et al. (1995) who suggested the quenching caused by the perturbed
276 | molecules during their transitions from several vibrational levels. Winds also affect the OH
277 | response to gravity waves and therefore they will also contribute to the spread of values seen
278 | between the various observation studies (e.g., Sonnemann G. and M. Grygalashvyly, 2003).

279 | Note that our observations as well as ~~models-simulations~~ show the phase Φ for OH to be
280 | a negative value indicating upward propagating waves (see Tarasick and Shepherd, 1992a, b). In

281 general we note that our Φ values, although on some occasions are closer to Viereck and Deehr
282 (1989) observations, show deviations from other investigators and are larger than the model
283 values on most occasions. Differences in theory and observation may be due to the horizontal
284 wavelength assumed in the model and or the Prandtl number (ratio of kinematic viscosity to
285 thermal diffusivity) assumed. The Prandtl number is important in theoretical calculations and
286 modeling, especially when in terms of dissipating waves owing to molecular viscosity and
287 thermal diffusivity while they propagate in the atmosphere (Hickey 1988). An error in the
288 Prandtl number assumption will affect the derived wave parameters (λ_z , η etc.), which ~~will~~may
289 ~~successively-in-turn result in mask the actual ones~~misleading results. In this regard, Makhlof et
290 al. (1995) studied the variations in the η values by modifying the model proposed by Hines and
291 using a photochemical dynamical model; however, they were still unable to explain the
292 appearance of the negative phases appropriately. Hines and Tarasick (1987) found a wide range
293 of η variability, a result supported by our measurements. Further, Hines and Tarasick (1997)
294 subsequently discussed the necessary correction for thin and thick layer approximations for the
295 calculation of η from airglow emissions due to gravity waves interaction. They also pointed out
296 that OH emission intensity, which affects the derived η values, does not depend on the oxygen
297 profile and other minor species, which contradicts the theory of Walterscheid et al. (1994),
298 Schubert et al. (1991). The calculated vertical wavelengths (VW) for all the nights of the
299 observation are shown in Figure 2c as pink half filled squares indicating the estimates for the
300 year 2010 and olive half filled squares for the year 2011. Large differences exist from one night
301 to another. The VW has a large variability ranging from -41 km to -102 km (2010) and -36.2
302 km to -140 km (2011) for long period waves, and, -26 to -92.4 and -24 to -88 km for short
303 period waves period of 2010 and 2011 years, respectively. In 2010 (and 2011) years, the mean

304 VW values for long and short period waves are calculated to be -60.2 ± 20 km (-77.2 ± 40 km)
305 and -42.8 ± 15 km (-59.2 ± 30 ~~km~~), respectively. Further, unlike the clear dependency on the
306 wave period noted in the Krassovsky parameters (η and Φ) no clear trend is noted in the
307 calculated VW. We also plot the values reported by Reisin and Scheer (1996) and Lopez-
308 Gonzalez et al. (2005) for a comparison. It is noteworthy that for all the days the VW for the
309 long period wave are higher than the VW of short period waves. We also observed that VW
310 values calculated for -2011 year are larger than 2010 year calculated values. We note that the
311 values reported by Reisin and Scheer (1996) are approximately -30 km with about 40 km
312 variability, ~~which Our values are is n~~ a good agreement with ~~our values~~ them. However, Lopez-
313 Gonzalez et al. (2005) observed VW values to be approximately -10 km deduced from their OH
314 observations, which do not agree with our values. Further, Ghodpage et al. (2012) analyzed the
315 long-term nocturnal data of 2004-2007 and also observed that the VW lies between 28.6 and 163
316 km. Recently, Ghodpage et al. (2013) studied the simultaneous mesospheric gravity wave
317 measurements in the OH emission from Gadanki and Kolhapur, inferring mean VWs varying
318 from -26 to -60 km for the Kolhapur observations. Takahashi et al. (~~2011~~1990) reported
319 vertical wavelengths varying from 20 to 80 km, which is in agreement with our values.

320

321 **4. Comparison with the Full Wave Model Results**

322 Wave simulations were performed using the Full Wave Model (FWM) for which the
323 representative inputs were taken for the duration of observations reported in section 3. The
324 observations were conducted over an approximate one month period spanning February 8th and
325 March 13th, and accordingly we used the middle date of this observation period (February 25th)
326 in the MSIS model to represent the ~~undisturbed~~ mean state. The latitude used was 16.8° N, and

327 the local time was midnight. Because the speed and direction of wave propagation were not
328 determined from the observations, several simulations were performed for each wave period in
329 which the direction of propagation (eastward, northward and westward propagation) and the
330 phase speed (50 m/s, 100 m/s and 150 m/s) were varied. Note that the mean winds (not shown) in
331 these simulations were derived from the Horizontal Wind Model (HWM) using the same input
332 parameters as used for the MSIS model. The derived meridional winds (not shown) are far
333 smaller than the zonal winds for the conditions considered here, and so while results for eastward
334 and westward propagation differed quite markedly, those for northward and southward
335 propagation did not. Hence we considered only a single direction (northward) for meridional
336 propagation.

337 We also performed a tidal simulation using an equivalent gravity wave model (Lindzen
338 1970; Richmond 1975), as implemented in an earlier study (Walterscheid and Hickey 2001).
339 The horizontal wavelength and Coriolis parameter are adjusted to give maximal correspondence
340 with a given tidal mode. Here, we performed calculations for the terdiurnal (3,3), (3,4), (3,5) and
341 (3,6) modes using parameters provided by Richmond (1975). The simplifications inherent in this
342 approach are discussed by Walterscheid and Hickey (2001).

343 Comparisons between the full wave model results for η , Φ and λ_z and the values inferred
344 from the observations are shown in figure 3a, 3b and 3c, respectively. In figure 3a we compare
345 the observed values of η for 2010 and 2011. The observed values of η are represented as pink
346 and olive lower half-filled squares for 2010 and 2011, respectively. In figure 3a we note that at
347 few of the longer wave periods, the observed values of η are in good agreement with the full
348 wave model results. For short period waves the values of η inferred from the observations appear

349 to be bounded by the model values for waves with horizontal phase velocities are 50 and 100
350 m/s, respectively. For example, for 3.6 hr wave periods, the average of the values of η inferred
351 from the observations is 3.7, while the full wave model values lie between about 0.5 (for the 100
352 m/s wave) and 7 (for the 50 m/s, eastward propagating wave). For the 8 hr wave periods, the
353 average of the values of η inferred from the observations is 5.7, which is bounded by the full
354 wave model estimates for waves having a horizontal phase velocity of 50 m/s and different
355 propagation directions.

356 Overall, we note that the comparison between the observed η values and the modeled
357 values can be explained by gravity waves whose horizontal phase velocities range from 50 m/s to
358 | 100 m/s. In this regard, an earlier investigation by ~~Pragati-Sikha et al. (2010) reported~~ observed
359 gravity wave horizontal phase speeds (for periods 5 min to 17 min) varying between 10 m/s and
360 48 m/s. The propagation directions were reported to be preferentially towards the north. More
361 recently, Taori et al. (2013) studied mesospheric gravity wave activity in the OH and OI 558 nm
362 emissions from Gadanki. They observed that the gravity waves were moving in the north-west
363 direction. The average phase velocity of the ripple-type waves was found to be 23.5 m/s. The
364 other, band-type waves, with horizontal scales of about 40 km, were found to be propagating
365 from south to north with an estimated phase speed of 90 m/s.

366 The vertical wavelengths (λ_z) calculated using the observed values of η and Φ differ
367 significantly from the full wave model estimate for waves with phase velocities below 100 m/s.
368 More typically, a comparison between those values inferred from the observations and those
369 derived from the model tend to agree for phase velocities in the 100 - 150 m/s range. However, it
370 should be noted that vertical wavelengths inferred from the observations are based on the use of
371 | the inferred Krassovsky's ratio, η , in Eq. (2). ~~Please n~~Note that the errors in the determination of

372 the phase (Φ) of η may lead to significant errors (proportional to $\cot\Phi$) in the determination of
373 λ_z , especially as Φ approaches $\pm 180^\circ$.

374 The differences noted in the observed and modeled estimates of Krassovsky ratio
375 magnitudes η and phase (Φ) may be associated with the limitation arising due to dynamics as
376 well as the measurements. In terms of measurements limitation, the parameters achieved with the
377 best fit method may have leaked contribution from other wave components, which may be
378 dynamically varying within a wave period. In terms of dynamics, that full wave model uses
379 climatological density (both major gas and minor airglow-related species) and wind profiles,
380 which will introduce uncertainties. This point has been previously elaborated by Walterscheid et
381 al. (1994) with respect to the effect of a change in the [O] profile on the OH response to wave
382 motions.

383 It is interesting to note that the arithmetic mean values of $|\eta|$ for the years 2010 and 2011
384 were 4.4 and 5.7 respectively. When we look at each $|\eta|$ value from one wave period range to
385 other, the difference is found to be more than 30% which is well above the maximum errors in
386 the estimation. One may further argue that this difference may not be significant. For this, we
387 looked at the mode of the values for periods ranges 1-4 hr, 4-6 hr, 6-8 hr and 8-10 hr. We found
388 that in each case in the year 2011 mode values are larger than the year 2010. The differences
389 noted in the magnitude of the observed Krassovsky ratio η between 2010 and 2011 may be
390 associated with variations in the height and shape of the undisturbed OH emission profile. We
391 use the SABER data to investigate this aspect. To check whether there was a difference in the
392 OH emission layer structure, we selected the nighttime OH emission profile for a grid
393 encompassing 10°N to 20°N latitudes and 70°E to 90°E latitudes during February, March and
394 April months of the years 2010 and 2011. We have selected the February to March period

395 because the optical airglow data used in this study was acquired primarily during these months.
396 | The monthly mean values of OH emission rates are ~~plotted-shown~~ in Figure 4. The solid curves
397 | correspond to 2010 data while the dashed curves correspond to 2011 data. We note that the peaks
398 | of OH emission layer during February, March and April of 2010 occurred at 84.2 km, 82.8 km
399 | and 85.1 km altitude, respectively, while the corresponding peaks for 2011 were found to occur
400 | at 85.8 km, 85.6 km and 85.2 km altitude. This suggests that the peak of the emission layer
401 | occurred at a somewhat lower altitude in 2010 compared to 2011. Also, the ~~e~~mission rates during
402 | February and March were found to be higher in 2010. It is important to note that in an earlier
403 | study, Ghodpage et al. (2013) compared the Krassovsky ratios at two different latitudes, Gadanki
404 | (13.5 N, 79.2E) and Kolhapur (16.8°N and 74.2°E) and noted a lower OH emission layer peak
405 | over Kolhapur and also larger estimated η values over Kolhapur. In the present case, instead of
406 | the location, it is the difference in the measurement year where the peak emission altitudes of the
407 | OH emission layer are somewhat different. As the peak emission layer arise due to the chemical
408 | reactions involving odd oxygen, it is proposed that chemical-~~constituents~~ composition was
409 | different from the year 2010 to the year 2011. Therefore, ~~the-noted~~modified OH emission rates
410 | may be responsible for the observed differences in the Krassovsky parameters. A further
411 | question that arise here is why the peaks should be different from one year to the other. As these
412 | months are pre-monsoon, when a large scale oscillation namely, El Niño/Southern Oscillation
413 | (ENSO) sweeps through the south Asian continent, we looked at the ENSO strength based on the
414 | Multivariate ENSO Index (MEI). This index is shown in table 1, where it is noteworthy that the
415 | MEI index for 2010 (January to May) is of opposite sign to that for the corresponding months in
416 | 2011. We postulate that these large scale processes have a profound impact on the observed
417 | wave energetics and dynamics at mesospheric altitudes. Large scale processes induced the wave

418 oscillations associated with the ENSO. The ENSO generates a spectrum of waves which are of
419 planetary scales. These are expected to generate a secular variation in temperature and density
420 structure throughout the atmosphere. A difference in ENSO suggests that these forcing are
421 different in the two years (2010, ~~and~~ 2011). At present, we do not know through which process
422 the ENSO may have implications in the observed wave characteristics. However, we believe that
423 further investigation is required in order to confirm whether or not any such associations really
424 do exist.

425

426 **5. Conclusion:**

427 We report the Krassovsky parameters for the observed gravity waves from Kolhapur (16.8°N and
428 74.2°E) and their comparison with the full wave model.

429 1) ~~It is evident that~~ The observed values of Krassovsky parameters in our study show a
430 large spread in their distribution as compared to the model values (shown in Figure 2a). A
431 similar spread in the distribution has also been reported by other investigators. We have
432 also observed magnitude of η values is larger in the year 2011 than 2010.

433 2) ~~It is also notable that~~ The values of η for the OH data in our study lie between the model
434 estimates and the values ~~observed by other investigators~~ reported in other published
435 results. Whereas the phase values are more than the model values on most occasions. We
436 note that our Φ measurements match with those reported by Viereck and Deehr (1989),
437 while they show large differences with ~~the other investigators~~ values in other reports.

438 3) Observed vertical wavelength (VW) values broadly agree with the range reported by
439 other investigators and are found to vary from -26 to -140 km. We also noted that VW

440 values calculated for 2011 year are larger than 2010 year calculated values. Most of
441 wave propagating upward in direction.

442 4) Comparison of observed η and Φ values agree fairly well with the full wave model
443 results for waves with 50 and 100 m/s horizontal phase velocities. Vertical wavelengths
444 tend to agree for waves with 100 and 150 m/s horizontal phase velocities, except for the
445 longest period waves for which vertical wavelength cannot be reliably inferred from the
446 observations.

447 | The database used in the present study ~~is~~are limited in terms of the length (time and duration)
448 and locations. Based on the above conclusions we emphasis that more rigorous study using
449 coordinated observations and modeling are required to uncover the physics occurring at upper
450 mesosphere.

451

452

453 **Acknowledgements**

454 This work is carried out under the research grant funded by Ministry of Science and Technology
455 and Department of Space, Govt. of India. RNG thank the Director, Indian Institute of
456 Geomagnetism (IIG), Navi Mumbai for encouragement to carry out this work. The night airglow
457 observations at Kolhapur were carried out under the scientific collaboration program (MoU)
458 between IIG, Navi Mumbai and Shivaji University, Kolhapur. MPH acknowledges the support of
459 NSF grant AGS-1001074.

460

461 **6. References**

462 | Aushev, V. M., Lyahov, V. V., Lopez-Gonzalez, M. J., Shepherd, M. G., and Dryna, E. A.:
463 | Solar eclipse of the 29 March 2006: results of the optical measurements by MORTI over
464 | Almaty (43.03°N, 76.58°E), *J. Atmos. Sol. Terr. Phys.*, 70, 1088–1101, 2008.

465 | Bruce, G. H., Peaceman, D. W., Rachford, Jr., H. H., and Rice, J. D.: Calculations of unsteady-
466 | state gas flow through porous media, *Petrol. Trans. AIME*, 198, 79-92, 1953.

467 | Bittner, M., Offermann, D., Graef, H. H.: Mesopause temperature variability above a
468 | midlatitude station in Europe. *Journal of Geophysical Research*, 105(D2): 2045–2058, 2000.

469 | Drob, D. P.: Ground-based optical detection of atmospheric waves in the upper mesosphere and
470 | lower thermosphere, Ph. D. Thesis, University of Michigan, Ann Arbor, MI., 1996.

471 | Ghodpage, R. N., Singh, D., Singh, R. P., Mukherjee, G. K., Vohat, P., and Singh, A. K.: Tidal
472 | and gravity waves study from the airglow measurements at Kolhapur (India), *J. Earth Syst.*
473 | *Sci.*, 121, 6, 1511–1525, 2012.

474 | Ghodpage, R. N., Taori, A., Patil, P. T., and Gurubaran, S.: Simultaneous mesospheric gravity
475 | wave measurements in OH night airglow emission from Gadanki and Kolhapur – Indian low
476 | latitudes, *Currents Science*, 104, 1, 98-105, 2013.

477 | Ghodpage, R. N., Taori, A., Patil, P. T., Gurubaran, S., Sharma, A. K., Nikte, S., and Nade, D.:
478 | Airglow Measurements of Gravity Wave Propagation and Damping over Kolhapur (16.8° N,
479 | 74.2° E), *International Journal of Geophysics (IJG)*, Volume 2014,1-9,
480 | <http://dx.doi.org/10.1155/2014/514937>, 2014.

481 | Greet, P. A., French, W. J. R., Burns, G. B., Williams, P. F. B., Lowe, R. P., ~~and~~ & Finlayson, K.
482 | : OH (6-2) spectra and rotational temperature measurements at Davis, Antarctica, *Annales*
483 | *Geophysicae*, 16(1), 77–89, 1998.

484 | Guharay, A., Taori, A., Bhattacharjee, B., Pant, P., Pande, P., and Pandey, K.: First ground-
485 | based mesospheric measurements from central Himalayas, *Current Science*, 97, 664-669,
486 | 2009.

487 | Guharay, A., Taori, A., and Taylor, M.: Summer-time nocturnal wave characteristics in
488 | mesospheric OH and O₂ airglow emissions, *Earth Planets Space*, 60, 973–979, 2008.

489 | Hecht, J. H., ~~Walterscheid, R. L., Christensen, A. B. and Pranke, J. B. et al.~~: Observations of
490 | wave-driven fluctuations of OH nightglow emission from Sondre Stromfjord, Greenland, *J.*
491 | *Geophys. Res.*, 92, 6091-6099, 1987.

492 | Hedin, A. E.: Extension of the MSIS thermosphere model into the middle and lower
493 | atmosphere, *J. Geophys. Res.*, 96, 1159 – 1172, 1991.

494 | Hickey, M. P., and Yu, Y.: A full-wave investigation of the use of a “cancellation factor” in
495 | gravity wave-OH airglow interaction studies, *J. Geophys. Res.*, 110, A01301,
496 | doi:10.1029/2003JA01372, 2005.

497 | Hickey, M. P., Huang, T.-Y., and Walterscheid, R.: Gravity wave packet effects on chemical
498 | exothermic heating in the mesopause region, *J. Geophys. Res.*, 108(A12), 1448,
499 | doi:10.1029/2002JA009363, 2003.

500 | Hickey, M. P., Walterscheid R. L., and Schubert, G.: Gravity wave heating and cooling in
501 | Jupiter’s thermosphere, *Icarus*, 148, 266-281, 2000.

502 Hickey, M. P., Walterscheid, R. L., Taylor, M. J., Ward, W., Schubert, G., Zhou, Q., Garcia, F.,
503 Kelley, M. C., and Shepherd G. G.: Numerical simulations of gravity waves imaged over
504 Arecibo during the 10-day January 1993 campaign, *J. Geophys. Res.*, 102, 11,475-11,489,
505 1997.

506 Hickey, M.P., Schubert, G., and Walterscheid, R. L.: Gravity wave-driven fluctuations in the O₂
507 atmospheric (0-1) nightglow from an extended, dissipative emission region, *J. Geophys.*
508 *Res.*, 98(13),717-730, 1993.

509 Hickey, M. P.: Effects of eddy viscosity and thermal conduction and coriolis force in the
510 dynamics of gravity wave driven fluctuations in the OH nightglow, *J. Geophys. Res.*, 93,
511 4077, 1988.

512 | Hickey, M. P., Taylor, M. J., Gardner, C. S., and Gibbons, C. R.: -Full-wave modeling of small-
513 scale gravity waves using Airborne Lidar and Observations of the Hawaiian Airglow
514 (ALOHA-93) O(1S) images and coincident Na wind/ temperature lidar measurements, *J.*
515 *Geophys. Res.* 103, 6439-6453,1998.

516 Hickey, M. P., and Cole, K. D.: A quartic dispersion equation for internal gravity waves in the
517 thermosphere, *J. Atmos. Terr. Phys.*, 49, 889-899, 1987.

518 Hines, C. O.: A fundamental theorem of airglow fluctuations induced by gravity waves, *J.*
519 *Atmos. Sol. Terr. Phys.*,59, 319–326, 1997.

520 Hines, C. O., and Tarasick, D. W.: Layer truncation and the Eulerian/ Lagrangian duality in the
521 theory of airglow fluctuations induced by gravity waves, *J. Atmos. Sol. Terr. Phys.*, 59, 327–
522 334, 1997.

523 | Hines, C. O., and Tarasick, D. W.: On the detection and utilization of gravity waves in airglow
524 | studies, *Planet Space Sci.*, 35, 851–866, 1987.

525 | Krassovsky, V. I.: Infrasonic variation of OH emission in the upper atmosphere, *Ann. Geophys.*,
526 | 28, 739–746, 1972.

527 | Lindzen, R. S.: Internal gravity waves in atmospheres with realistic dissipation and temperature,
528 | part I: Mathematical development and propagation of waves into the thermosphere, *Geophys.*
529 | *Fluid Dyn.*, 1, 303-355, 1970.

530 | Lindzen, R. S., and Kuo, H. L.: A reliable method for the numerical integration of a large class
531 | of ordinary and partial differential equations, *Mon. Wea. Rev.*, 97, 732-734, 1969.

532 | Liu, A. Z., and Swenson, G. R.: A modeling study of O₂ and OH airglow perturbations induced
533 | by atmospheric gravity waves, *J. Geophys. Res.*, 108, D4, 4151, doi:10.1029/2002JD002474,
534 | 2003.

535 | Lopez-Gonzalez, M. J., [Rodriguez, E., Shepherd, G. G., Sargoytchev, S., Shepherd, M. G.,](#)
536 | [Aushev, V. M., Brown, S., Garcia-Comas, M., and Wiens, R. H. et al.](#): Tidal variations of O₂
537 | Atmospheric and OH(6-2) airglow and temperature at mid-latitude from SATI observations,
538 | *Ann. Geophys.*, 23, 3579–3590, 2005.

539 | Makhlof, U. B., Picard, R. H., and Winick, J. R.: Photochemical-dynamical modeling of the
540 | measured response of airglow to gravity waves, 1: basic model for OH airglow, *J. Geophys.*
541 | *Res.*, 100, 11,289–11,311, 1995.

542 | Mies, F. H.: Calculated vibrational transitions probabilities of OH ($X^2\pi$). *Journal of —Molecular*
543 | *Spectroscopy*, 53, 150–188, 1974.

544 | Meinel, A. B.:OH Emission bands in the spectrum of the night sky I. ~~American Geophysical~~
545 | ~~Union, 31 (21),~~Astrophys. J., 111, 555 – 564, 1950.

546 | Meriwether, J. W.: High latitude airglow observations of correlated short term fluctuations in the
547 | hydroxyl Meinel 8-3 band intensity and rotational temperature, Planet. Space Sci., 23, 1211–
548 | 1221, 1975.

549 | Oznovich, I., Walterscheid, R. L., Sivjee, G. G., and McEwen, D. J.: On Krassovsky’s ratio for
550 | ter-diurnal hydroxyl oscillations in the winter polar mesopause, Planet Space Sci.,45(3), 385–
551 | 394, 1997.

552 | Oznovich, I., McEwen, D. J., and Sivjee, G. G.: Temperature and airglow brightness oscillations
553 | in the polar mesosphere and lower thermosphere, Planet Space Sci., 43, 1121–1130, 1995.

554 | Pragati, R.S., Parihar, N., Ghodpage, R., Mukherjee, G.K.: Characteristics of gravity waves in
555 | the upper mesosphere region observed by OH airglow imaging, Current Science 98, 392–397,
556 | 2010.

557 | Reisin, E.R., and Scheer, J.: Vertical propagation of gravity waves determined from zenith
558 | observations of airglow, Adv. Space Res. 27(10), 1743-1748, 2001.

559 | ~~Reisin, E. R., and Scheer, J.: Gravity wave activity in the mesopause region from airglow~~
560 | ~~measurements at El Leoncito, J. Atmos. Sol. Terr. Phys., 66, 655–661, 2004.~~

561 | Reisin, E. R., and Scheer, J.: Characteristics of atmospheric waves in the tidal period range
562 | derived from zenith observations of O₂(0-1) Atmospheric and OH (6-2) airglow at lower mid
563 | latitudes, J. Geophys. Res., 101, 21,223–21,232, 1996.

564 Richmond, A. D.: Energy relations of atmospheric tides and their significance to approximate
565 methods of solution for tides with dissipative forces, *J. Atmos. Sci.*, 32, 980-987, 1975.

566 Schubert, G., Hickey, M. P., and Walterscheid, R. L.: Heating of Jupiter's thermosphere by the
567 dissipation of upward propagating acoustic waves, *Icarus*, 163, 398-413, 2003.

568 | Schubert, G., Walterscheid, R. L., and Hickey, M. P.: Gravity wave-driven fluctuations in OH
569 | nightglow from an extended, dissipative emission region, *J. Geophys. Res.*, 96 (A8), 13,869–
570 | 13,880, 1991.

571 | Sivjee, G. G., &and Hamwey, R. M.: Temperature and chemistry of the polar mesopause OH.
572 | *Journal of Geophysical Research*, 92(A5): 4663–4672, 1987.

573 Stubbs, L. C., Boyd, J. S., and Bond, F. R.: Measurement of the OH rotational temperature at
574 Mawson, East Antarctica, *Planet. Space Sci.*, 31 (8), 923–932, 1983.

575 | Sonnemann, G. and Grygalashvyly, M.: The zonal wind effect on the photochemistry within the
576 | mesosphere / menopause region, *Adv. Space Res. Vol. 32 (5)*, 719-724, 2003.

577 Takahashi, H., Buriti, R. A., Gobbi, D., and Batista, P. P.: Equatorial planetary wave signatures
578 observed in mesospheric airglow emissions, *J. Atmos. Sol. Terr. Phys.*, 64, 1263–1272, 2002.

579 Takahashi, H., Sahai, Y., Batista, P. P., and Clemesha, B. R.: Atmospheric gravity wave effect
580 on the airglow O₂(0-1) and OH (9-4) band intensity and temperature variations observed from
581 a low latitude station, *Adv. Space Res.*, 12(10), 131–134, 1992.

582 Takahashi, H., Sahai, Y., and Teixeira, N.R.: Airglow intensity and temperature response to
583 atmospheric wave propagation in the mesopause region, *Adv. Space Res.* 10, (10)77-(10)81,
584 1990.

585 ~~Tarasick, D. W. and Hines, C. O.: The observable effects of gravity waves in airglow emission,~~
586 ~~Planet. Space Sci., 38, 1105–1119, 1990.~~

587 Takahashi, H, Batista, P. P, Buriti, R. A, Gobbi, D, Nakamura, T, Tsunda, T ~~&-and~~ Fukao, S.:
588 Simultaneous measurements of airglow OH emission and meteor wind by a scanning photometer
589 and the MU radar. Journal of Atmospheric and Solar-Terrestrial Physics, 60(17): 1649–1668,
590 1998.

591 Tarasick, D. W. and Hines, C. O.: The observable effects of gravity waves in airglow emission,
592 Planet. Space Sci., 38, 1105–1119, 1990.

593 Taylor, M. J., Gardner, L. C., –and Pendleton, Jr. W. R.: Long-period wave signatures in
594 mesospheric OH Meinel (6,2) band intensity and rotational temperature at mid-latitudes, Adv.
595 Space Res., 27(6–7), 1171– 1179, 2001.

596 Taylor, M. J., Turnbull, D. N., and Lowe, R. P.: Coincident imaging and spectrometric
597 observations of zenith OH nightglow structure, Geophys. Res. Lett., 18, 1349–1352, 1991.

598 Taori, A., and Taylor, M. J.: Characteristics of wave induced oscillations in mesospheric O2
599 emission intensity and temperatures, Geophys. Res. Lett., 33, L01813,
600 doi:10.1029/2005GL024442, 2006.

601 Taori, A., Taylor, M. J., and Franke, S.: Terdiurnal wave signatures in the upper mesospheric
602 temperature and their association with the wind fields at low latitudes (20°N), J. Geophys.
603 Res., 110, D09S06, doi: 10.1029/2004JD004564, 2005.

604 | Taori, A., Jayaraman, A., and Kamalakar, V.: Imaging of mesosphere–thermosphere airglow
605 | emissions over Gadanki (13.5°1N, 79.2°4E)-first results, *J. Atmos. Sol. Terr. Phys.* 93, 21–
606 | 28, <http://dx.doi.org/10.1016/j.jastp.2012.11.007>, 2013.

607 | Tarasick, D. W., and Shepherd, G. G.: Effects of gravity waves on complex airglow chemistries:
608 | 1. O₂(b¹Σ_g⁺) emission, *J. Geophys. Res.*, 97, 3185–3193, 1992a.

609 | Tarasick, D. W., and Shepherd, G. G.: Effects of gravity waves on complex airglow chemistries:
610 | 2. OH emission, *J. Geophys. Res.*, 97, 3195–3208, 1992b.

611 | Vargas, F., Swenson, G., Liu, A., and Gobbi, D.: O(¹S), OH, and O₂(b) airglow layer
612 | perturbations due to AGWs and their implied effects on the atmosphere, *J. Geophys. Res.*, 112,
613 | D14102, doi:10.1029/2006JD007642, 2007.

614 | Viereck, R. A., and Deehr, C. S.: On the interaction between gravity waves and the OH Meinel
615 | (6-2) and O₂Atmospheric (0-1) bands in the polar night airglow, *J. Geophys. Res.*, 94, 5397–
616 | 5404, 1989.

617 | Walterscheid, R. L., and Schubert, G.: Dynamical-chemical model of fluctuations in the OH
618 | airglow driven by migrating tides, stationary tides, and planetary waves, *J. Geophys. Res.*,
619 | 100, 17,443–17,449, 1995.

620 | Walterscheid, R. L., and Hickey, M. P.: -One-gas models with height-dependent mean molecular
621 | weight: Effects on gravity wave propagation, *J. Geophys. Res.*, 106, 28,831-28,839, 2001.

622 | Walterscheid, R. L., Schubert, G., and Hickey, M. P.: -A Comparison of Theories for Gravity
623 | Wave Induced Fluctuations in Airglow Emissions, *J. Geophys. Res.*, 99, 3935, 1994.

624 Walterscheid, R. L., Schubert, G., and Hickey, M. P.: Comparison of theories for gravity wave
625 fluctuations in airglow emissions, *J. Geophys. Res.*, 99, 3935–3944, 1994.

626 Walterscheid, R. L., Schubert, G., and Straus, J. M.: A dynamical chemical model of wave-
627 driven fluctuations in the OH nightglow, *J. Geophys. Res.*, 92, 1241 – 1254, 1987.

628

629

630

631 **Figure captions:**

632 **Figure 1.** Nocturnal variability in the mesospheric OH emissions on 26-27 January 2011. The
633 upper panels represent the mean deviations in (a) intensity and (b) temperature data. Bottom
634 panels represent (c) intensity and (d) temperature residuals. Solid line curves in each plot show
635 the result of simple best-fit cosine model.

636

637 **Figure 2 (a)** ~~A comparison~~Distribution of Krassovsky parameter ' η ', ~~s of data to their respective~~
638 ~~wave periods reported by investigators (list not exhaustive).~~ The x -axis shows the wave
639 periodicity and the y-axis is for amplitude of Krassovsky parameters (η ~~and Φ~~) ~~in each plot. A~~
640 ~~close resemblance between the observational values and discrepancy between the observational~~
641 ~~and theoretical estimates are notable.~~ The legends in the figure are as following: (~~η : 1 (for 2010~~
642 ~~year) & 2 (for 2011 year);~~ present study ; 3, Schubert et al. 500 km; 4, Schubert et al. 1000 km;
643 5, Tarasick and Shepherd 500 km; 6, Tarasick and Shepherd 1000 km; 7, Takahashi et al. (1992);
644 8, Oznovich et al. (1995); 9, Drob et al. (1996); 10, Reisin and Scheer (1996); 11, Taylor et al.
645 (2001); 12, Guharay et al (2008); 13, Walterscheid and Schubert (1995); 14, Lopez-Gonzalez et
646 al. (2005); 15, Oznovich et al. (1997)); 16, Viereck and Deehr (1989).

647 **Figure 2 (a1)** Observed values of η ~~verses versus~~ wave period over Kolhapur alone.

648 **Figure 2 (b)** ~~A comparis~~Distribution of phi phase values of Krassovsky parameter ' Φ ', reported
649 by investigators (list not exhaustive) to their respective wave periods (~~Φ : 1 (for year 2010); & 2~~
650 ~~(for year 2011);~~ present study; 3, Schubert et al. 500 km; 4, Schubert et al. 1000 km; 5, Tarasick
651 and Shepherd 500 km; 6, Tarasick and Shepherd 1000 km; 7, Viereck and Deehr (1989); 8,
652 Oznovich et al. (1995); 9, Drob et al. (1996); 10, Reisin and Scheer (1996); 11, Taylor et al.

653 (2001); 12, Guharay et al.(2008); 13, Walterscheid and Schubert (1995); 14, Lopez-Gonzalez et
654 al. (2005); 15, Oznovich et al. (1997); 16,Viereck and Deehr (1989);).

655 **Figure 2 (b1)** Observed values of Φ verses wave period over Kolhapur alone.

656 **Figure 2(c)** Deduced vertical wavelength (VW) for both the short and long period wave as
657 function of wave periodicity compared to other published results. ~~Also shown comparison with~~
658 ~~values obtained by other investigators.~~

659 **Figure 3(a)** Comparison with η calculated by observation of both year and Full wave model
660 simulation with their respective wave period. Pink and olive lower half filled square shows the
661 2010 and 2011 year η observations (1 and 2 present study η ; 3,FWM simulation of η for 50 m/s
662 horizontal phase velocity; 4, FWM simulation of η for 100 m/s horizontal phase velocity; 5,
663 FWM simulation of η for 150 m/s horizontal phase velocity).

664 **Figure 3(b)** Simillar ~~as to~~ figure 3(a) but for phase values for both the short and long period
665 wave. **Figure 3(c)** Simillar ~~to as~~ figure 3(a) but for deduced vertical wavelength (VW).

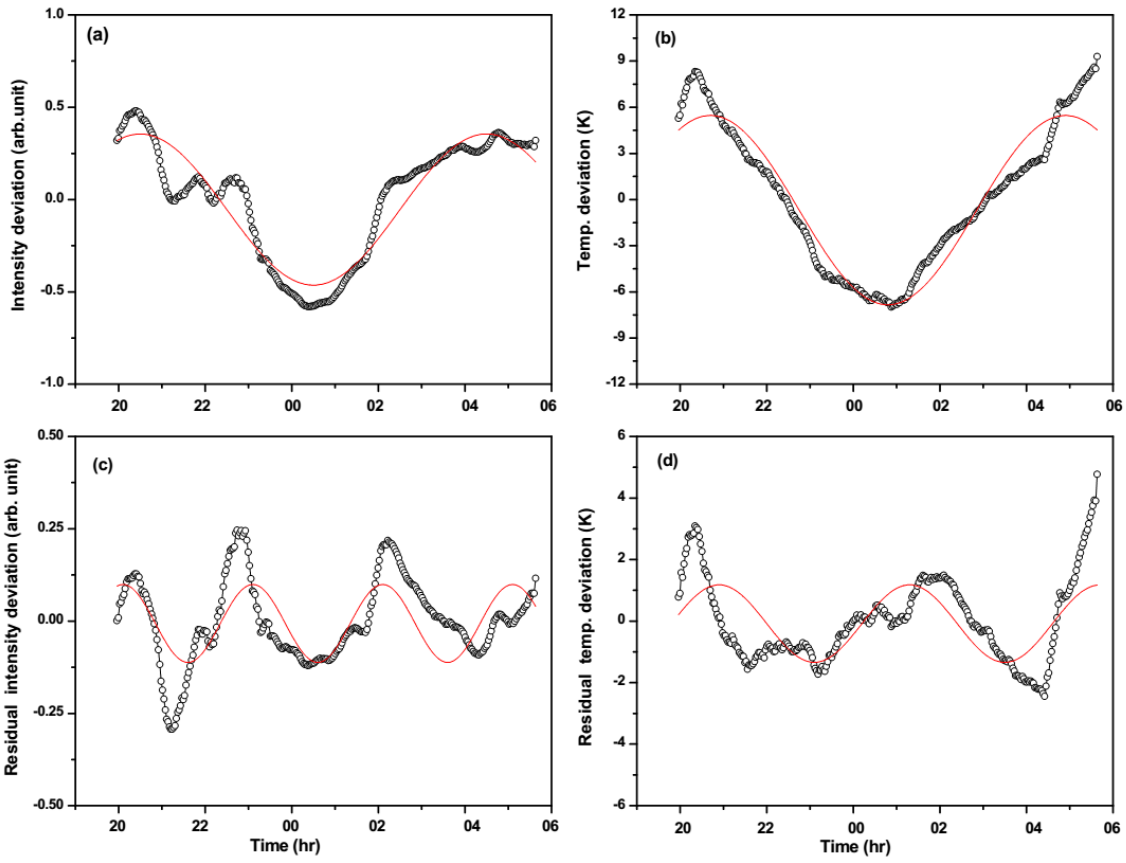
666 **Figure 4.** The monthly (February, March and April) mean ~~values of~~ OH emission rates ~~are~~
667 profiles from SABER for the year 2010 (solid lines) and 2011 (dashed lines). ~~shown in plot (~~
668 ~~which are obtain from SABER data).~~ ~~The solid lines plot the data for the year 2010 while the~~
669 ~~dashed lines represent the year 2011.~~

670

671 **Table 1.** Comparisons of deduced wave parameters in 2010 and, 2011 years with MEI index and
672 OH altitudes. The observed quantities are mean for their representative wave periods. (JFM-
673 January, February and March months like this)

674

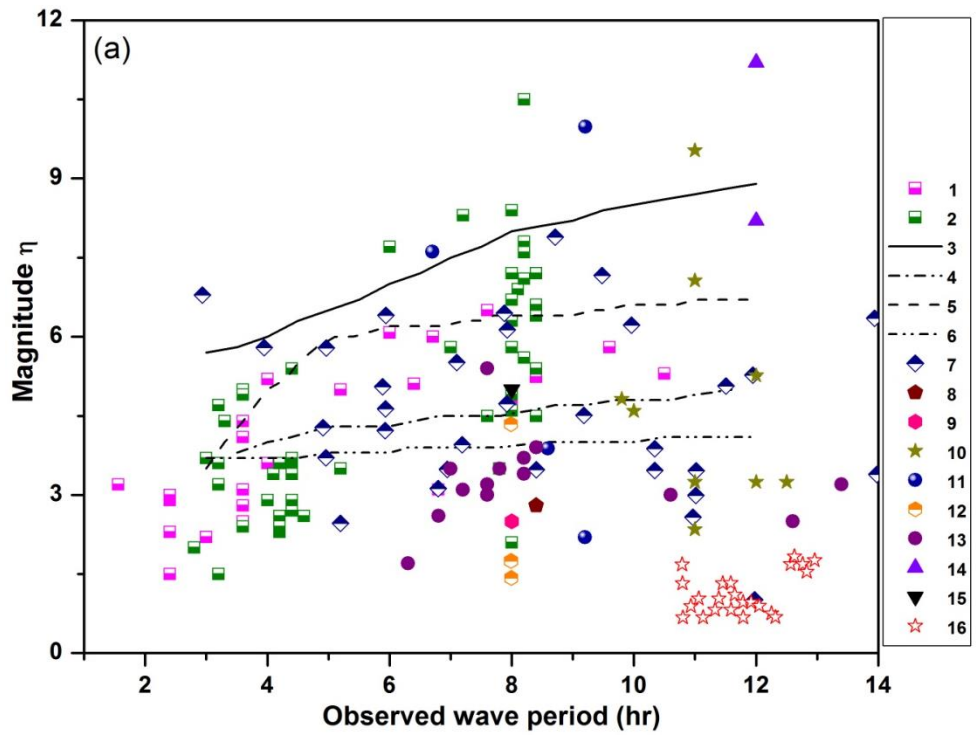
26 - 27 January 2011; Kolhapur



675

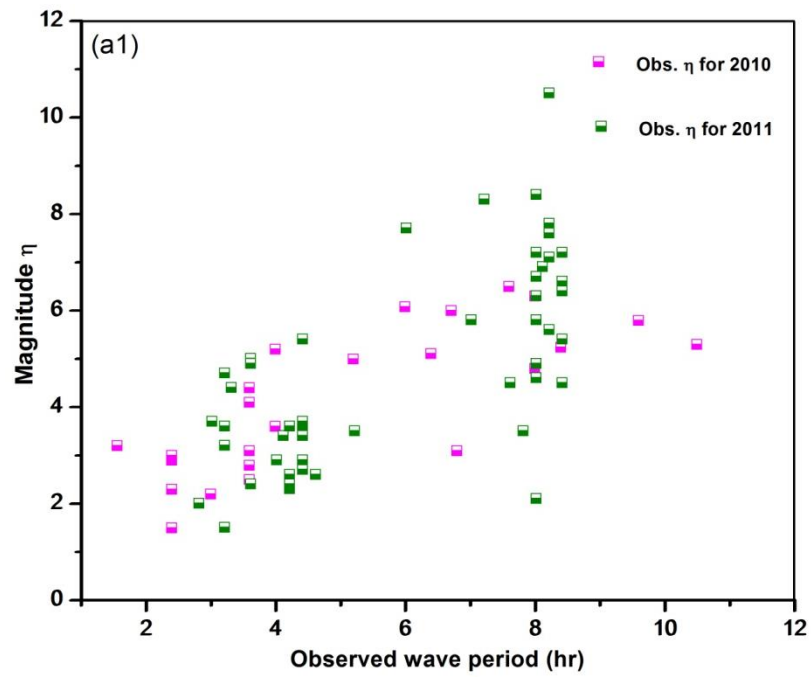
676 Figure 1.

677



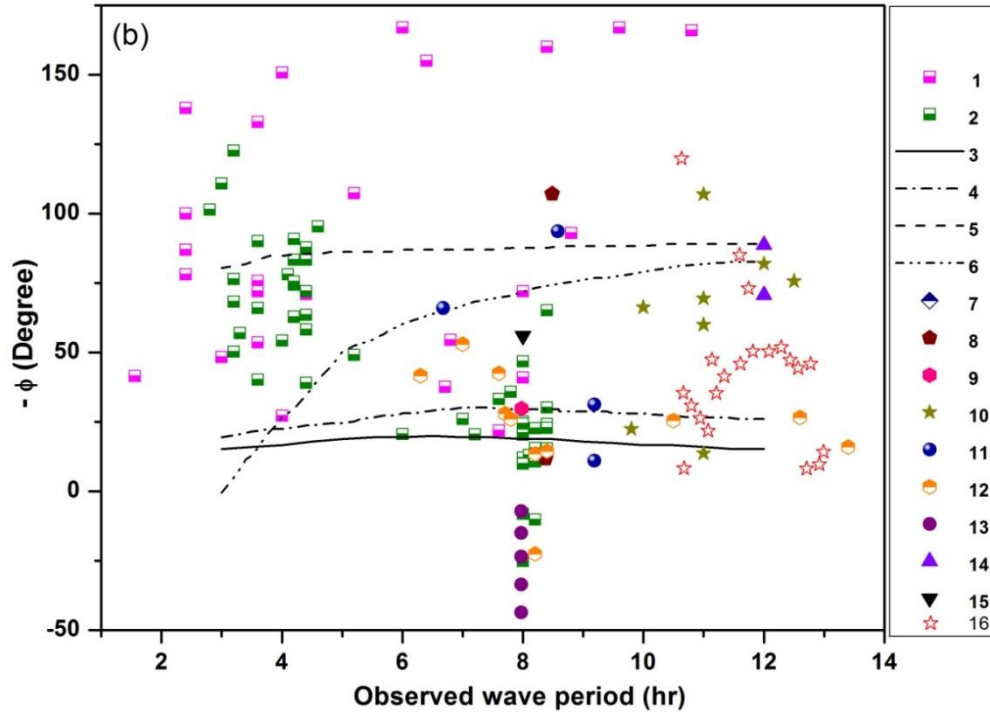
678

679 Figure 2(a)

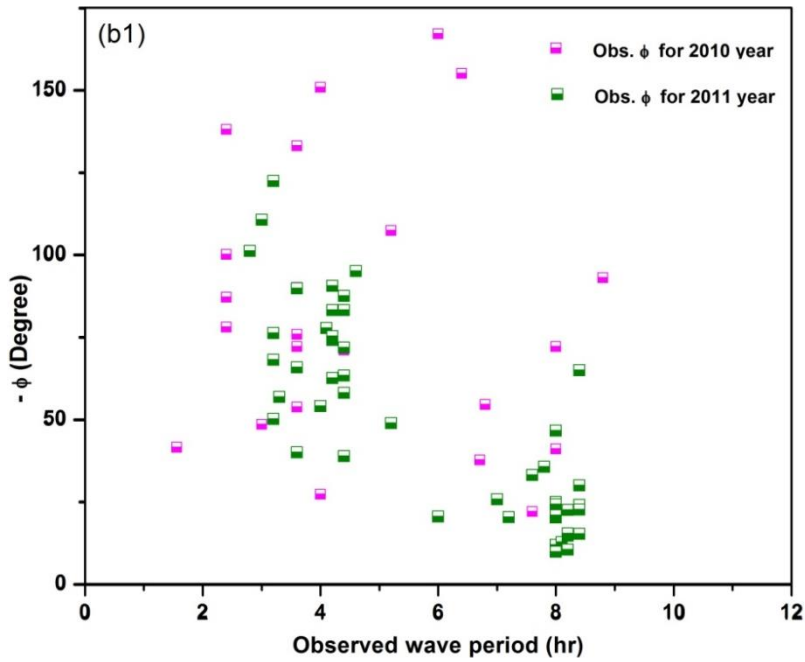


680

681 Figure 2(a1)



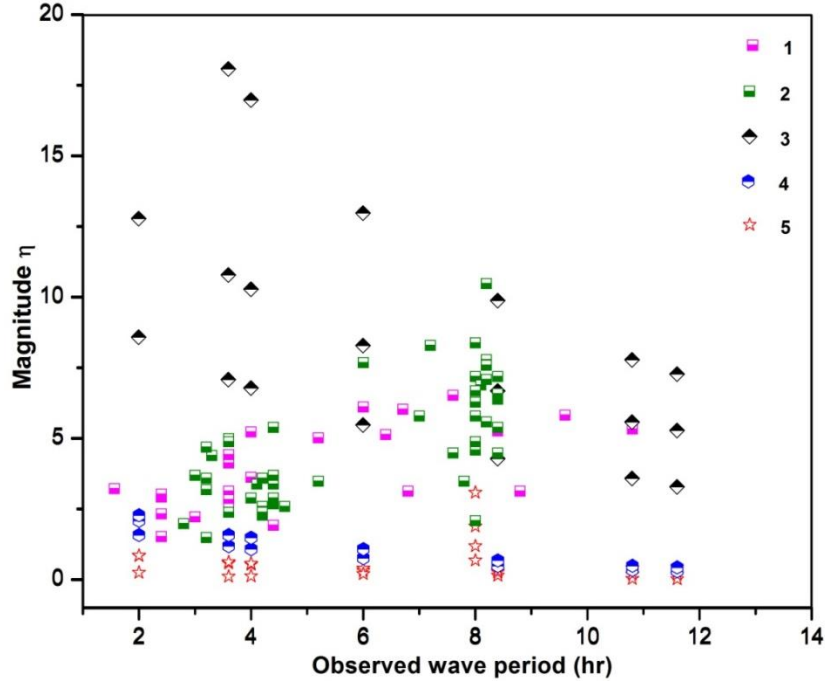
683 Figure 2(b)



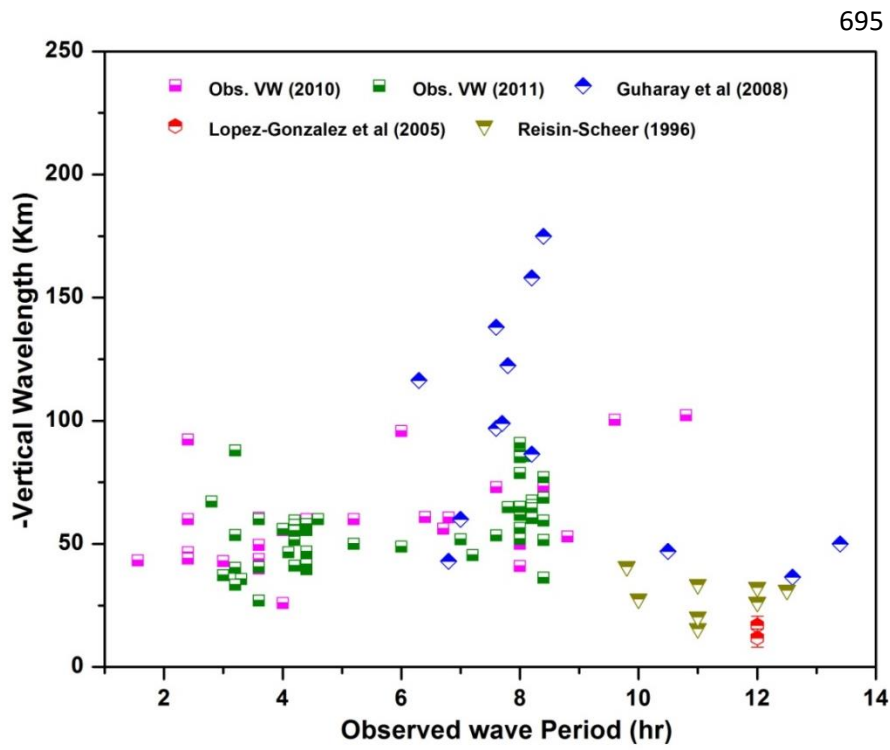
685

686 Figure 2(b1)

687

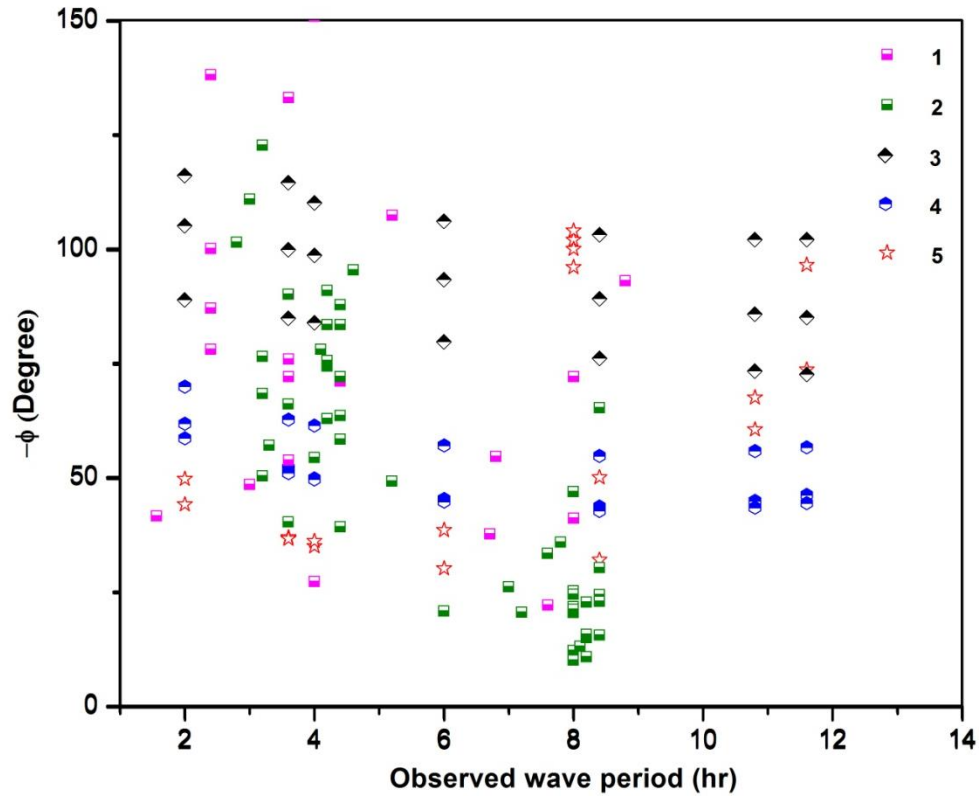


694 Figure 2(c)



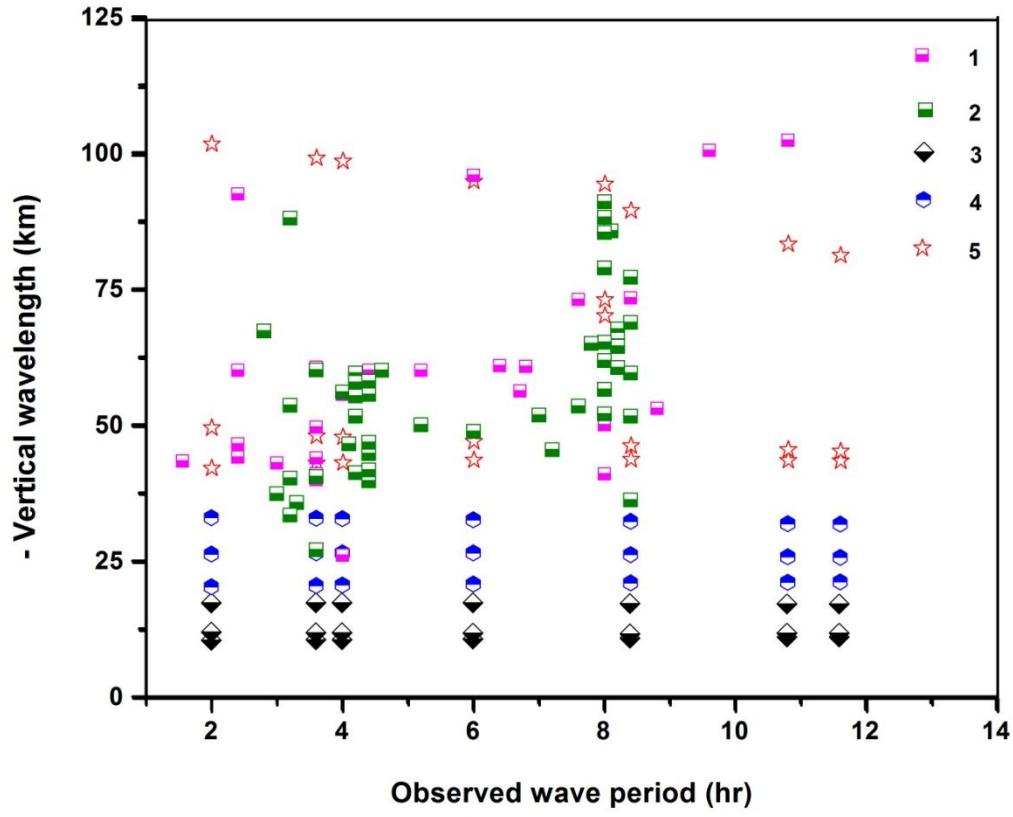
696

697 Figure (3a)



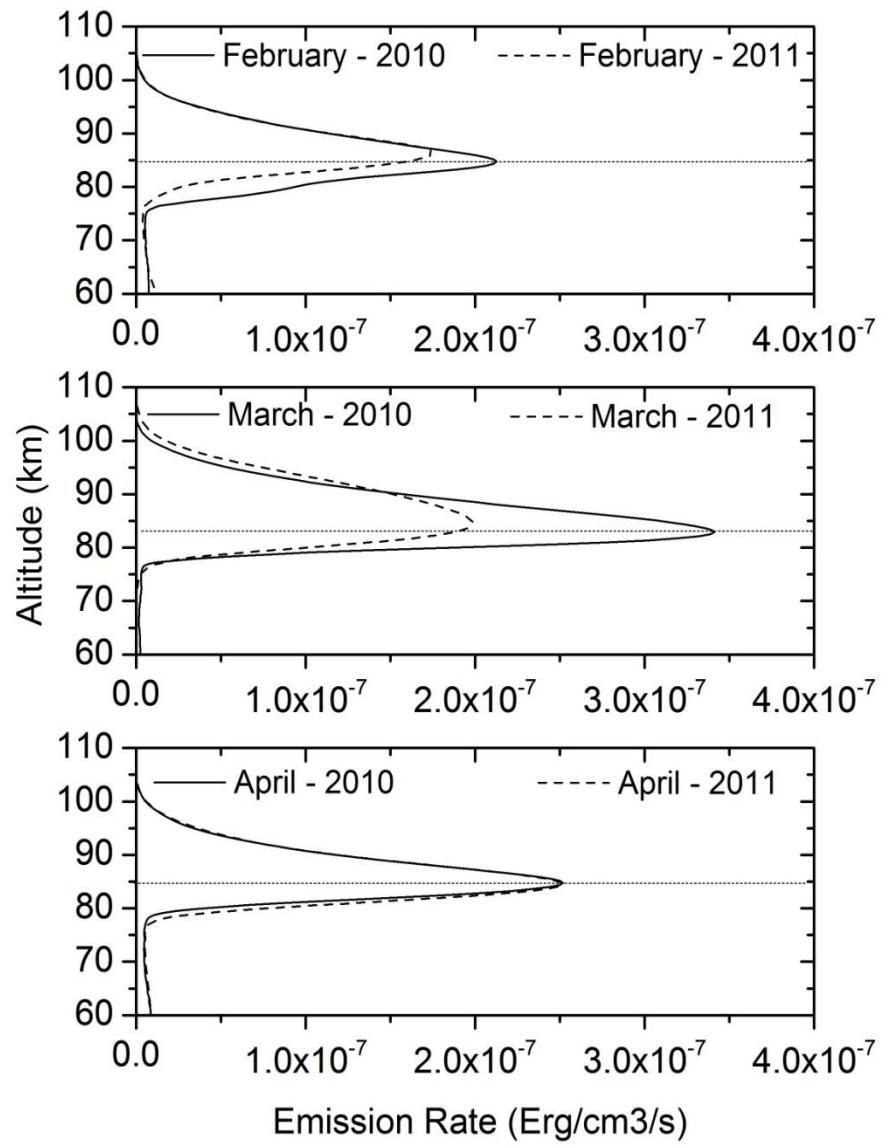
698

699 | Figure 3(b)



700

701 Figure 3 (c)



702

703 Figure 4.

704

705

706

707

708

709 Table 1.

Year	Mean η (\pm Errors)		Mean ($-\Phi$) (Deg.)		Mean ($-VW$) (km)		OH altitude (km)	MEI index				
	Long wave period	Short wave period	Long wave period	Short wave period	Long wave period	Short wave period		JFM	FMA	MAM	SON	OND
2010	4.4 \pm 1	2.3 \pm 0.9	90.6 \pm 40	70.4 \pm 45	60.2 \pm 20	42.8 \pm 15	82 km to 85.1 km during February – April	1.1	0.8	0.5	-1.4	-1.3
2011	5.7 \pm 1.7	2.7 \pm 0.6	33.8 \pm 40	64.4 \pm 40	77.6 \pm 40	59.2 \pm 30	85.1 km to 86 km during February – April	-1.1	-0.8	-0.6	-0.9	-0.9

710

711